Optimal floating offshore wind farms for Mediterranean islands

Renewable Energy 221 (2024) 119785

Contents lists available at ScienceDirect

Renewable Energy

journal homepage: www.elsevier.com/locate/renene

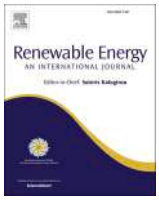

Optimal floating offshore wind farms for Mediterranean islands

E. Faraggiana *, A. Ghigo, M. Sirigu, E. Petracca, G. Giorgi, G. Mattiazzo, G. Bracco

Department of Mechanical and Aerospace Engineering, Polytechnic University of Turin, 10129, Torino, Italy

ARTICLE INFO

Keywords:
Renewable energy
Wind farm
Offshore
Floating platform
Optimisation

ABSTRACT

Offshore wind will play an important role in achieving the Green Deal's goals of green transition and renewable energy generation. The European Union (EU) has launched an initiative to support a clean energy transition towards sustainable and renewable energy production in the EU islands. In fact, the Mediterranean islands obtain most of their energy supply from imported fossil fuels, making electricity costs generally very high due to their remote location. In this paper, we compare the optimal offshore wind farm layout, type and number of wind turbines for four selected sites next to Mediterranean islands. Each layout is evaluated in terms of levelised cost of energy, taking into account aerodynamic wake and transmission losses in the productivity estimation and a detailed cost model. Aerodynamic losses are modelled using a Jensen kinematic wake model and an area overlapping model to consider partial wake shadowing between wind turbines, while transmission losses are estimated as Ohmic losses of the inter-array and export transmission cables. Compared to the state-of-the-art PyWake code, the in-house MATLAB wake model demonstrated higher computational efficiency and is integrated into an efficient optimisation algorithm consisting of several iterations of the Interior-point optimisation algorithm. Results show that offshore wind turbines can provide renewable energy at a competitive price, especially at the most energetic site with an LCOE about 80 €/MWh. The normalised optimal LCOE and capacity factor as a function of the number of wind turbines are not significantly influenced by the chosen location and reach a maximum difference of 2–3 %, showing that they mainly depend on the type of wind turbine. The lowest optimal LCOE depending on the number of wind turbines is reduced by about 10 % and 25 % by the higher rated wind turbine.

1. Introduction

The energy transition towards more sustainable and secure energy production from renewable sources will reduce dependence on fossil fuels, which are generally only available in a few countries around the world. Island communities can particularly benefit from an independent energy system, as they are often isolated and not connected to the mainland grid. Their energy planning is often complicated as seasonal fluctuations in electricity demand due to tourism activities are high and require oversizing of renewable energy plants and energy storage such as Battery Energy Storage Systems (BESS) and Pumped Hydro Energy Storage (PHES) [1]. Grid flexibility can be improved by sector coupling strategies and Demand Side Management solutions. Hydrogen Energy Storage (HES) is particularly effective when coupled with the transport sector, e.g. through power-to-transport solutions [2]. Various European projects such as H2Ocean, MERMAID, and TROPOS have investigated the integration of HES from marine renewable energy produced by multi-use platform concepts [3–5]. However, the techno-economic feasibility of HES in offshore wind farm projects has not yet been reached, although it could become more competitive in the long term by increasing the carbon tax [6,7].

A renewable energy mix is usually required to diversify renewable energy technologies and reduce the fluctuation of energy produced, for example by combining renewable energy from wind and solar, which have different seasonal patterns. An optimal energy mix can be optimised in particular to reduce the Levelised Cost of Energy (LCOE) [8]. Solar photovoltaics (PV) is generally chosen in the energy mix of Mediterranean island communities [9]. However, the available area for onshore renewable energy technologies is generally limited, while the Marine Renewable Energy (MRE) potential in the Mediterranean Sea is high and still needs to be exploited [10,11]. Floating PV systems are also a solution for the offshore environment, but they are mostly deployed in calm waters

* Corresponding author.
E-mail addresses: emilio.faraggiana@polito.it (E. Faraggiana), alberto.ghigo@polito.it (A. Ghigo), massimo.sirigu@polito.it (M. Sirigu), ermando.petracca@polito.it (E. Petracca), giuseppe.giorgi@polito.it (G. Giorgi), giuliana.mattiazzo@polito.it (G. Mattiazzo), giovanni.bracco@polito.it (G. Bracco).

https://doi.org/10.1016/j.renene.2023.119785
Received 15 March 2023; Received in revised form 25 November 2023; Accepted 5 December 2023
Available online 9 December 2023

characterised by the absence of waves and currents [12,13]. Offshore wind is likely to be the most prominent MRE technology in the near future. However, offshore wind potential in the Mediterranean is particularly constrained by bathymetry, limited wind resources and the minimum distance from the coast required by local legislation to reduce visual impact. In fact, the Mediterranean seabed quickly becomes deep at greater distances from the coast, which reduces the technical feasibility of bottom-fixed offshore wind farms in particular. Despite this challenge, the offshore wind potential in the Mediterranean Sea is large and is estimated at 4629 TWh (EU electricity demand in 2021 was 2865 TWh), with the majority (99 %) coming from floating offshore wind energy, as bottom-fixed offshore wind is limited to a restricted area in the Adriatic Sea [11]. Some studies have focused on wind farm site assessment for Mediterranean Islands [14–17]. In Ref. [14] a spatial resource assessment analysis was carried out to identify the main suitable sites for the major Mediterranean islands including Sardinia, Cyprus, and Malta. In Refs. [15, 16] the offshore wind potential was estimated for the Greek islands of Samothrace Island and Crete respectively. In Ref. [17], the spatial distribution of offshore wind farms was optimised for the Corsica island in order to reduce the temporal fluctuations of wind power.

A wind farm project faces several challenges to minimise aerodynamic losses and optimise the cost of energy. Therefore, it is essential to optimise the wind turbine positions to maximise the energy production of the wind farm [18,19]. Far wake models such as the Jensen' model are a good choice for optimising the wind farm layout, as they offer a good trade-off between computational time and accuracy. It has been shown that a non-uniform optimised wind farm layout provides higher energy production than uniform layouts [20–22]. Meta-heuristic optimisation algorithms are extensively used due to their ability to optimise complex optimisation problems characterised by multiple local optima. Mosetti et al. [20] solved the wind farm layout problem using a genetic algorithm (GA), maximising the power produced by the wind farm and minimising the installation cost. Grady et al. [21] replicated the same methodology of Mosetti et al. [20], but modified the settings of the GA to improve the results. In Ref. [23], a binary real-coded genetic algorithm was shown to provide better optimal configurations for a large range of number of wind turbines (10–50). These GA approaches are based on a discrete solution space, which is based on a limited number of possible positions, since the layout space is constantly discretised as a grid. A continuous layout space leads to nonlinear constraints as the wind turbines cannot be placed too close to each other. A first attempt to solve the nonlinear optimisation problem was made by Ozturk and Norman using a greedy heuristic approach [22]. In Ref. [24], a bi-objective evolutionary strategy algorithm was used to solve the constrained nonlinear optimisation problem. In particular, all constraints were embedded in an objective function that was minimised during the optimisation.

Other optimisation algorithms that were used to optimise the wind farm layout were the Simulated Annealing algorithm (SA) [25,26], the Particle Swarm Optimisation (PSO) [27,28] and the Ant Colony Optimisation [29]. In Ref. [25], it was found that as the wind turbine density increases, the optimised layout slightly improves the power production as the wake effects become more homogeneous within the wind farm area. In Ref. [26], both SA and GA were used to optimise the wind farm layout, with SA showing a higher convergence efficiency of the optimisation. The PSO proved to be an efficient optimisation algorithm that improved the results of Mosetti and Grady [27] and showed better performance compared to GA and the evolutionary algorithm [28].

Multi-objective optimisation has also been used to obtain an optimal wind farm layout that considers both the wind farm power production and the cost of the configuration [30,31]. The main benefit of multi-objective optimisation for wind farm optimisation is that there is no clear preference between power and cost objective functions and a larger number of acceptable solutions can be chosen. In Ref. [32], a multi-objective optimisation was proposed maximising both wind farm power and efficiency.

Levelised Cost of Energy (LCOE) was included in the layout optimisation in Refs. [33–35]. In Ref. [34], the genetic and particle swarm algorithms were used to minimise the LCOE for the Middelgrunden wind farm considering the sub-optimisation of the electrical infrastructure. In Ref. [35], it was found that an optimal non-homogeneous wind farm produces a higher power production but has a higher LCOE compared to a homogenous wind farm with the largest wind turbine considered.

Mathematical programming has also been used to optimise wind farm layout [36–39]. In Ref. [36], quadratic integer and mixed integer linear programs were used to optimise the wind farm layouts. Compared to previous results by Mosetti et al. [20] and Grady et al. [21], a slightly more efficient and symmetric layout was obtained. In Ref. [37], a sequential global optimisation approach is presented to optimise the German offshore wind farm Alpha Ventus. The approach consists of repeating a heuristic initial solution and a mathematical programming technique.

Previous works show that optimising an offshore wind farm considering non-linear constraints and a continuous spatial domain is not a trivial task. Several optimisation algorithms have been used without a clear indication of the best optimisation algorithm for wind farm layout optimisation studies [20–29]. The influence of wind turbine type and site on optimal wind turbine layout and the inclusion of detailed techno-economic analysis in wind farm optimisation have also not been extensively investigated. In fact, wind farm optimisation studies have mainly optimised the wind farm power production and a simplified calculation of the total cost of the wind farm [20–31,36–39]. Few studies on layout optimisation have considered the LCOE, as it is difficult to accurately estimate the cost of the wind farm, and the influence of the number and type of wind turbines is generally not considered [33–35]. Wind farm layout optimisation for Mediterranean islands has not been addressed in previous studies [14–17] and is generally limited to the investigation of offshore wind potential. Compared to previous studies, this work investigates the optimal offshore wind farm layout for several Mediterranean islands and compares newly proposed efficient optimisation algorithms for wind farm layout optimisation. This study aims to provide an integrated tool to minimise the LCOE of an offshore wind farm layout and to investigate the influence of selected Mediterranean offshore sites, number, and type of wind turbines on the optimal LCOE. The methodology of the energy production and cost model and the results of this work will provide useful insights and details to developers and researchers regarding the optimal design of offshore wind farms for Mediterranean islands. Hybrid optimisation algorithm approaches combining deterministic and stochastic algorithms are proposed similar to Ref. [37] and compared with a modified genetic algorithm (mGA). A computationally efficient numerical model to estimate the annual energy production of the offshore wind farm is developed in MATLAB and compared with the DTU Pywake code [40], which increases the confidence in the model. More specifically, the annual energy production of the wind farm is estimated using the Jensen wake model, an area overlapping model, and the sum-of-squares wake interaction model (SS). The optimal wind farm layout is studied to minimise the electricity production costs by reducing both the aerodynamic losses and the grid connection costs between each turbine. The optimal normalised LCOE (nLCOE) and capacity factor (nCF) as a function of the number of wind turbines are similar for the different chosen locations, showing that they mainly depend on the wind turbine type. This is a significant result of this study, as a similar number of wind turbines minimising the LCOE for a given wind farm area can be installed at different offshore locations, which are easily influenced by wind energy resources, and can be used as a reference for wind energy developers.

Selected Mediterranean islands and metocean data are described in Section 2.1, while the wake modelling and floating wind turbine types used in this study are presented in Sections 2.2 and 2.3, respectively. The energy production calculation of the offshore wind farm, including aerodynamic and electrical losses, is shown in Section 2.4. The techno-

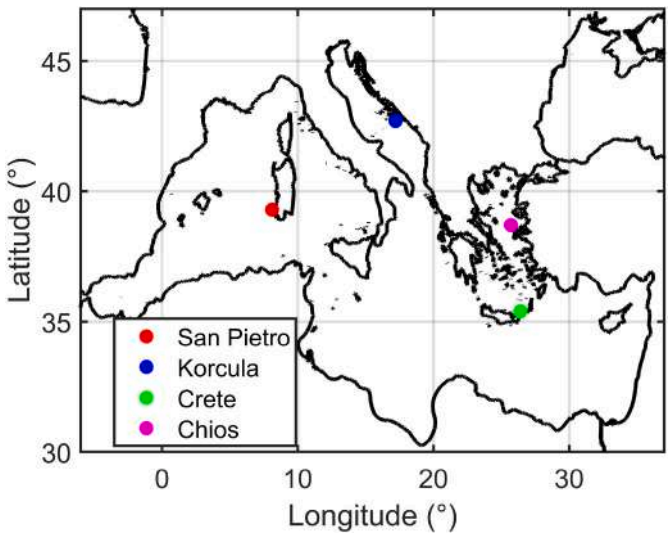

Fig. 1. Visualization of the selected sites.

economic model which is finalised to calculate the Levelised Cost of Energy (LCOE) is described in Section 2.5, while the assumptions for the optimisation layout and approach are presented in Section 2.6. The results show the verification of the model with Pywake in Section 3.1, the convergence of the optimisation in Section 3.2, and the optimal layout configurations for the Mediterranean islands in Section 3.3. Finally, the discussion and conclusion are presented in Sections 4 and 5.

2. Material and methods

2.1. Mediterranean islands

Many Mediterranean islands rely on fossil fuels for electric energy production and there is a need for a policy change towards a more sustainable and secure energy production. This study examines offshore wind farm solutions for several Mediterranean islands to support their energy transition [41].

The islands selected for this study have a population larger than 50000 people or are interconnected to the mainland, as the designed floating offshore wind farm requires a minimum electric load capacity. Four different islands with good potential for floating offshore wind were selected, namely San Pietro, Korcula, Crete, and Chios (See Fig. 1). These islands were chosen due to their location in the Mediterranean Sea for different Mediterranean countries, and due to technical constraints explained afterwards. Most of San Pietro's electricity comes from Sardinia via two submarine cables connected to the grid, and only a small part comes from photovoltaic plants [42]. Korcula is a Croatian island interconnected to the mainland via a submarine cable. The island aims to become carbon-free by 2050 and is therefore investing in sustainable energy production. Crete is the largest and most populated Greek island. Crete has recently been interconnected with Peloponnese, but diesel power plants are still used in the residential sector [16,43]. The island has a vast potential for offshore wind energy production especially on the eastern side, which is currently untapped. Chios is a Greek island not interconnected to the mainland and its electricity is mainly produced by diesel power plants, with only 11 % of total electricity produced coming from renewables. Chios is one of the major islands in the Mediterranean Sea with a clear interest in a clean energy transition and was therefore selected for this study [44].

Suitable sites are obtained considering several exclusion zones such as Natura 2000 sites, military areas, and shipping routes. Natura 2000 sites are an ecological network composed of sites from the Birds and Habitats Directives. These constraints were checked using the interactive map of the EMODnet website [45]. Other requirements for the installation of the wind farm, motivated hereafter, are the minimum distance to shore, which is assumed 20 km, a maximum depth of 1000 m, and a minimum wind speed of 6 m/s at 100 m (See Table 1). A minimum distance to shore is required to minimise the visual impact of the offshore wind farm, which is generally dependent on the size of the wind turbine. The maximum operating water depth is mainly limited by the increasing costs and challenges of longer mooring cables. The minimum wind speed is chosen as a reference because higher energy sites provide better results in terms of capacity factor and LCOE [19]. These constraints are similar to those chosen in the European Commission's report that analysed the offshore grid potential in the Mediterranean [11].

The distance to shore, the bathymetry, and the wind speed were obtained from the Global Wind Atlas and the New European Wind Atlas [46,47] and are listed in Table 2. The offshore wind farm sites were chosen 20 km from the coast, which is the minimum distance to minimise the offshore wind farm transmission line costs. The water depth is generally at or above 180 m for four of the selected sites and only Korcula has a shallower water depth (120 m). Wind speeds range from lower speeds in Korcula (6.2 m/s) to the most energetic sites in Chios and Crete (8.3 and 8.6 m/s, respectively). Finally, a maximum number of wind turbines is estimated for Chios, since it is a not interconnected island with a limited load capacity. Assuming a capacity factor of 40 % and an electricity consumption of 0.6 kW per person [48], the maximum allowable installed capacity is estimated to be 30.8 MW, corresponding to 15 and 5 of the 5 MW and 15 MW wind turbines types, respectively.

2.1.1. Wind data

Wind data were obtained from the New European Wind Atlas (NEWA), which provides hourly time series of wind speed and direction with a mesoscale resolution of 3 km × 3 km. Data are obtained for the years 2008–2018, the most recent decade available in the NEWA database, which is based on a WRF model and ERA5 reanalysis data, as the authors did not have field data available [49]. A higher number of wind directions and wind speeds of the Weibull distribution generally improves the accuracy of the annual energy production (AEP) estimation. However, many wind directions reduce the quality fit of the Weibull distribution as it reduces the number of wind speeds in each wind direction sector. In a previous study [37], it was suggested that 12 directions represent a good compromise between quality fit, wake effect errors, and computational time. In this study, a sensitivity analysis of the number of directions and the wind speed of the Weibull distribution is performed to investigate the influence on the accuracy of the AEP, as shown in Fig. 2. The sensitivity analysis considers a wind farm layout with 10 offshore wind turbines. The energy production of the offshore wind farm is represented with sufficient accuracy when the number of wind directions is 10 or greater, while the wind speed step (WSS) has only a minor impact on the wind farm productivity. Wind roses of each site and an example of Weibull distribution computation for San Pietro are represented in Fig. 3. Korcula is the site with the largest variability in wind direction, while on Crete the wind direction is mainly from a single direction (NW).

Table 1
Constraints of the offshore wind farm.

Population	Distance to shore (km)	Water depth (m)	Wind speed 100m (m/s)	Exclusion zones
>50000 or interconnected	≥ 20 km	<1000m	6	Protected and military areas, shipping routes.

Table 2
Selected islands for this study (Source: Global Wind Atlas + New European Wind Atlas + EMODnet).

Islands	Coord.	Pop.	Distance to shore (km)	Water depth (m)	Wind speed 100m (m/s)	Intercon.	Max. turb. (5 MW, 15 MW)
San Pietro (Italy)	[39.3N, 8.1E]	5,926	20	180	6.9	Yes	–
Korcula (Croatia)	[42.7N, 17.2E]	15,522	20	120	6.2	Yes	–
Crete (Greece)	[35.4N 26.4E]	617,360	20	300	8.6	No	–
Chios (Greece)	[38.7N, 25.7E]	51,390	20	270	8.3	No	15, 5

2.2. Wake modelling

Several wake models have been developed to predict the wake deficit of a wind turbine and to determine the aerodynamic power losses in a wind farm. A large number of models are based on the Navier-Stokes equations (e.g. k-ε and eddy-viscosity), but kinematic models are also very popular due to their lower computational time. Kinematic models only employ the momentum equation to model the velocity deficit of the wake. They have to be coupled with a turbulence model, especially for a more accurate load calculation [50]. The kinematic model used in this study is the Jensen model, also known as the PARK model [51,52]. It assumes a linearly expanding wake which depends only on the distance behind the rotor. The wake downstream will describe a cone with an expanding radius (r_W) of

$$r_W = r \cdot \left(1 + \frac{kx}{r}\right) = r \cdot (1 + 2ks) \tag{1}$$

where r is the radius of the rotor, k is the decay constant which depends on turbulence and atmospheric stability, x is the distance behind the rotor, and s is the relative distance behind the rotor $\left(\frac{x}{2 \cdot r}\right)$. The decay constant can be calculated as

$$k = \frac{0.5}{\ln\left(\frac{z}{z_0}\right)} \tag{2}$$

where z is the wind turbine's height and z_0 is the surface roughness of the wind farm area. z_0 is obtained from the Global Wind Atlas [46] and is equal to 0.0002 m in the offshore environment.

The wind farm is made of N_T wind turbines located at the following coordinates:

$$C = \begin{bmatrix} x1 & y1 \\ x2 & y2 \\ \dots & \dots \\ x_{N_T} & y_{NT} \end{bmatrix} \tag{3}$$

The velocity (u_{ij}) in the fully developed wake due to the turbine j at the location of a turbine i placed along the downstream of the wake is given as

$$u_{ij} = u_j \cdot \left(1 - \frac{2 \cdot a}{(1 + 2ks)^2}\right) = u_j \cdot \left(1 - \frac{1 - \sqrt{1 - c_T}}{(1 + 2ks)^2}\right) \tag{4}$$

where a is the axial induction factor and c_T is the thrust coefficient relative to the wind speed at the turbine j.

A rotor-average model is also considered to model the influence of the upstream wind turbine j when it partially shadows the downstream wind turbine i. The area overlapping model has been selected as it is an effective and simple model which has been chosen in previous wind farm optimisation studies [53]. The intersection area between the wake area at position x_i generated by the turbine j and the rotor area of turbine i (A_{ij}) is equal to [54]

$$A_{ij} = \begin{cases} 0 & d_{ij} \geq r_w + r \\ \pi \cdot r^2 & d_{ij} \leq r_w - r \\ r_w^2 \cos^{-1}\dfrac{d_1}{r_w} - d_1\sqrt{r_w^2 - d_1^2} + r^2 \cos^{-1}\left(\dfrac{d_2}{r}\right) - d_2\sqrt{r^2 - d_2^2} & r_w - r < d_{ij} < r_w + r \end{cases} \tag{5}$$

where

$$d_1 = \frac{r_w^2 - r^2 + d^2}{2d_{ij}} \tag{6}$$

and

$$d_2 = \frac{r_w^2 - r^2 + d^2}{2d_{ij}} \tag{7}$$

and d_{ij} is the distance between turbine i and j along the y axis.

The wind speed of a turbine i depends on the presence of all upstream wind turbines j and therefore it is fundamental to define a wake interaction model [39]. The wake interaction model used in this study is the Sum of Squares (SS), which has been demonstrated to be the most accurate [50,53]. This model is expressed by the following equation which is used to find the wind speed u_i for each wind turbine, taking into account all wake deficit from upstream wind turbines:

$$\left(1 - \frac{u_i}{u_\infty}\right)^2 = \sum_{j=1}^{N} \left(1 - \frac{u_{ij}}{u_j}\right)^2 \cdot \frac{A_{ij}}{A_r} \tag{8}$$

Finally, wind speed on each wind turbine is obtained for 10 discretised wind directions in order to calculate the AEP of the wind farm, which is explained in Section 2.4. Wind direction is identified with an angle θ relative to the North and requires a wind farm reorientation to obtain the x axis along the wind direction and wind turbine renumbering according to their position along the wind direction [37]. Therefore, the new coordinates are recalculated using the rotation matrix:

$$C' = \left(\begin{bmatrix} \cos(\theta) & -\sin(\theta) \\ \sin(\theta) & \cos(\theta) \end{bmatrix} C^T\right)^T \tag{9}$$

2.3. Floating wind turbine

Floating offshore wind turbines are generally selected for deep waters with a water depth higher than 60 m, as fixed-bottom offshore wind turbines are not economically feasible [55]. Several floating offshore wind turbines have been developed to reduce the overall cost of an offshore wind project [56]. Three major types have been developed by industry which are identified by the different design drivers to obtain the stability of the platform: buoyancy-stabilized, mooring-stabilized, and ballast-stabilized type of platforms. Each type has advantages and disadvantages related to the installation, mooring, floating platform

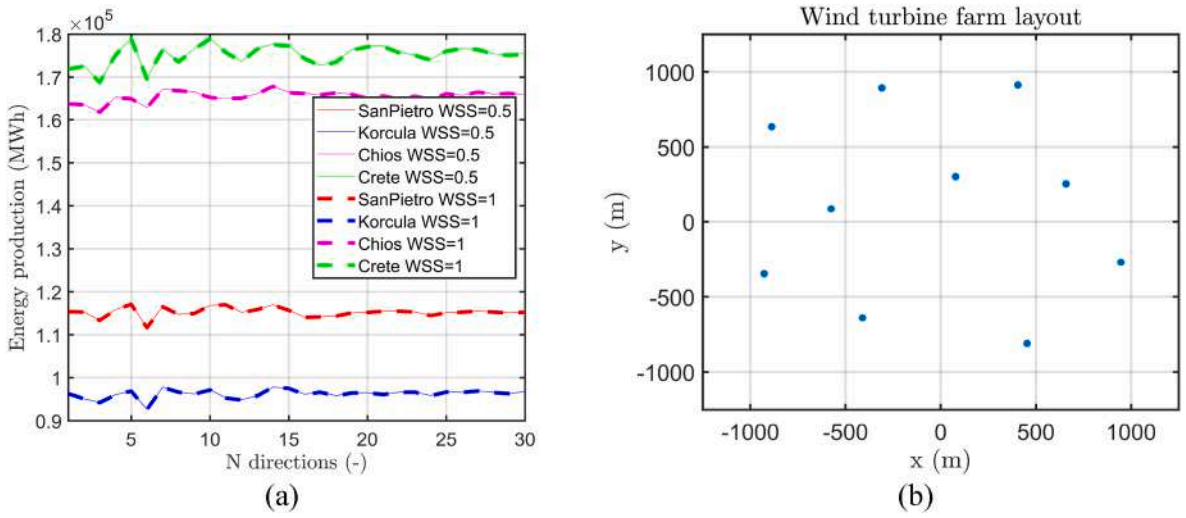

Fig. 2. Sensitivity of the energy production on the number of wind directions for two wind speed step (WPS) (a) for a 10 wind turbine layout (b) and the 5 MW wind turbine.

costs, and site location. The floating offshore wind turbines selected for this study are the Hywind [57] and WindFloat [58] floating offshore wind turbines (See Fig. 4), as they are good examples of the most developed and advanced TRL stage floating wind turbines. Hywind is a spar-type ballast-stabilized platform, and was selected for three of the different locations with the deepest water depth ($\geq$ 180 m). WindFloat is a semi-submerged platform and it was chosen for the Korcula offshore site in Croatia, which has a shallower water depth of 120 m, making the semi-submerged floating wind turbine more suitable than a spar. In fact, a spar type of platform requires a higher water depth due to the large draft [59].

The NREL 5 MW and the IEA 15 MW reference offshore wind turbine [60,61] were chosen for this study due to their widespread application in several research projects and their publicly available simulation models [62]. The wind turbine thrust coefficients and power values have been obtained from the steady-state of the OpenFAST simulations of the NREL 5 MW and the IEA 15 MW bottom-fixed offshore wind turbine, using version 2.5.0 of the ROSCO controller (See Fig. 5). Wind turbine thrust coefficients were capped at 1 because of the momentum conservation the Jensen model is based.

2.4. Offshore wind farm

For the inter-array grid connection of the offshore wind farm, a star configuration was chosen with the offshore substation placed in the center of the wind turbine farm. Compared to the radial network, this configuration has the advantage of having a separate circuit for each wind turbine, which can reduce power losses due to the failure and maintenance of each power cable [65].

It is assumed that the wind turbine can re-orient its rotor towards the incoming wind direction and that there are no power losses during the transient states. The annual energy production (AEP) of the wind farm can be obtained by discretising wind speed and wind direction:

$$AEP = 8760 \cdot \left(\eta_{avail} \sum_{\mathrm{n}=1}^{N_d} p_n \sum_{t=1}^{N_T} \int P_{wt}(u,n) \cdot p(u,\mathrm{n}) du - P_{losses} \right) \tag{10}$$

where N_d, N_T are the number of wind directions and wind turbines, p_n is the probability associated with the wind direction, $P_{wt}(u,n)$ is the power produced by turbine t for its corresponding wind speed u and wind direction n, $p(u,n)$ is the Weibull distribution, η_{avail} is the average availability of the offshore wind turbines which is assumed in this study as 95 % [33] and P_{losses} are the power electrical losses. The integral of the power curve and the Weibull distribution is made to estimate the mean power for each wind turbine and wind direction. The Weibull distribution is expressed as

$$p(u,\mathrm{n}) = k_n \frac{u^{k_n-1}}{c_n^{k_n}} e^{-\left(\frac{u}{c_n}\right)^{k_n}} \tag{11}$$

where k_n and c_n are the shape and scale parameters estimated for the wind speeds for each discretised wind direction section n. The Weibull distribution parameters are obtained from the timeseries of wind speed associated to each wind direction θ_n.

P_{losses} is calculated for the inter-array cables and the export cable considering Ohmic power losses and a constant power loss per unit length along the cable. This is generally a fair assumption for short cables less than 80 km [33]. The power losses are obtained as

$$P_{losses} = 3 \cdot \left(\sum_{i=1}^{N_T} R_{int_i} \cdot I_{int_i}^2 + R_{ex} \cdot I_{ex}^2 \right) \tag{12}$$

where R is the cable resistance, I is the grid current, the subscripts "*int*" and "*ex*" refers to inter-array and export cables respectively.

The cable resistance is obtained as

$$R = \frac{\rho_c \cdot L_c}{S_c} \tag{13}$$

where ρ_c is the copper resistivity of the cable $\left(1.75 \cdot 10^{-8}\ \frac{\Omega}{m}\right)$, L_c is the length of each cable segment and S_c is the cross-sectional area of the cable.

The current of each cable is obtained considering a three phase AC and can be expressed as follows [66]:

$$\mathrm{I} = \frac{P}{\sqrt{3} \cdot V \cos(\varphi)} \tag{14}$$

where P and V are the average power and voltage for each cable, $\cos(\varphi)$ is the power factor. A high power factor equal to 0.95 is assumed in this study for double-fed asynchronous generator according to Refs. [66,67].

The section cable (S_c) is obtained by imposing a maximum voltage drop percentage (1 %) and a maximum acceptable current. These values

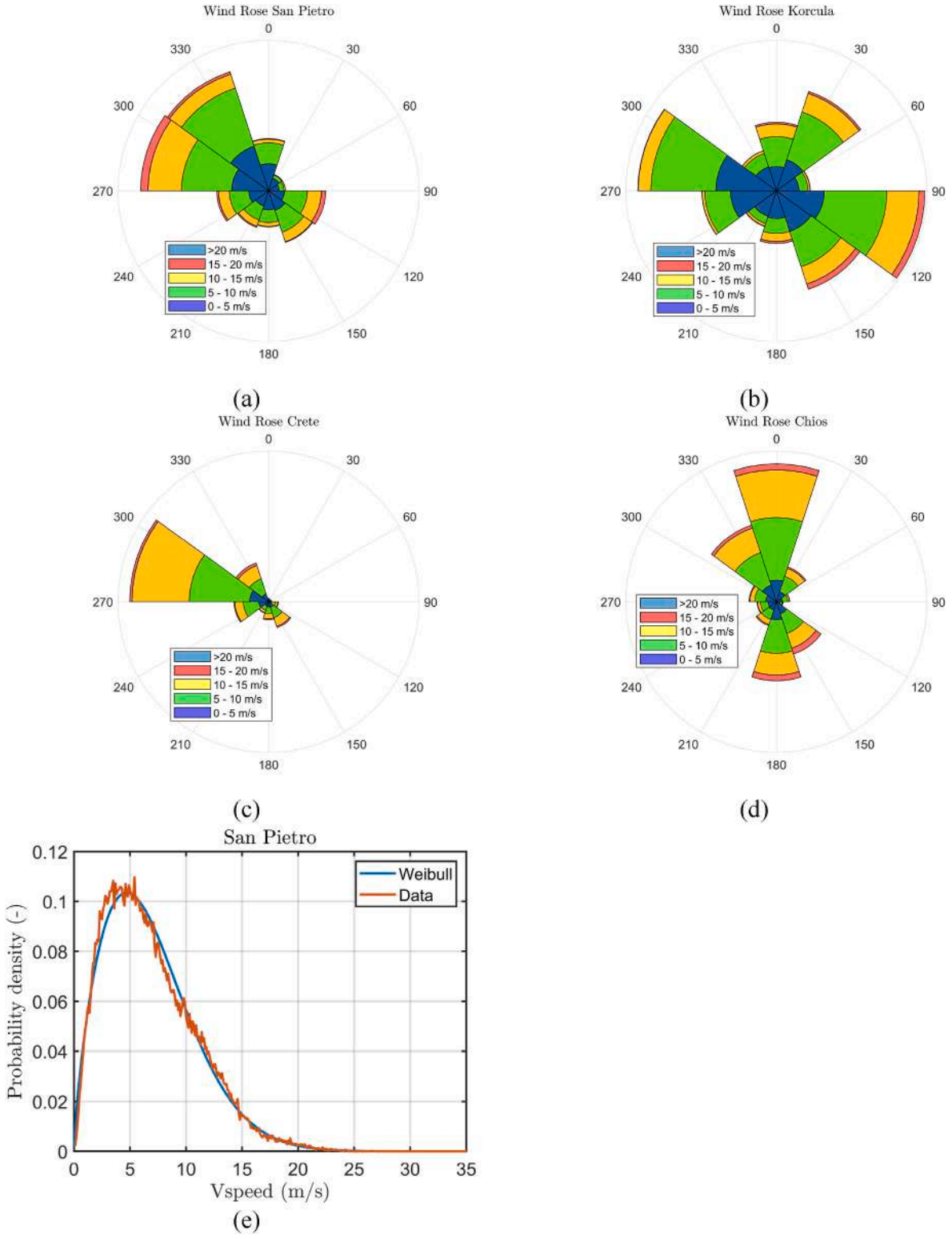

Fig. 3. Wind rose for ten wind directions (a–d) and Weibull distribution of San Pietro (e).

Fig. 4. Hywind (a) and WindFloat (b) floating offshore wind turbines [63,64].

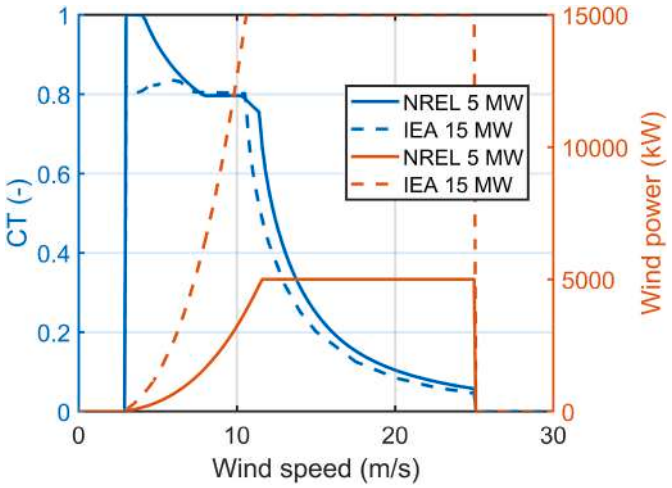

Fig. 5. Thrust coefficients (CT) and wind power of the NREL 5 MW and IEA 15 MW.

have been obtained from the IEC 60228 standard on conductors of insulated cables [68] and from the catalogue of marine cables available from Cable Service Srl [69]. Power cables selected in this study are 3-core XLPE cables, as they have low manufacturing costs and dielectric losses [65]. The voltage drop is calculated as

$$\Delta V = \sqrt{3} \cdot I_n \cdot L_c \cdot \frac{Z_c}{1000} \tag{15}$$

where Z_c is the impedance of the cable $\left(\frac{\Omega}{km}\right)$ which depends on the conductor resistance and reactance.

The maximum current (I_z) is obtained as follows [69]:

$$I_z = I_{z\ th} * k \tag{16}$$

where k is a correction factor based on the mean environmental temperature and $I_{z\ th}$ is the maximum current at a reference temperature for a specific S_c.

The selected cable cross-sectional area is the smallest section which respects a $\Delta V < 1$ % and $I_n < I_z$. The look-up tables of conductor resistance, correction factor (k), and maximum current (I_z) used in this study are shown in Fig. 6. The conductor reactance affects the cable impedance (Z_c) less than the conductor resistance for smaller cable sections (especially for sections less than 300 mm^2) and it is considered in a range between 0.01 and 0.15 Ω/km [69]. An example of a selected cross-section of the export cable for an offshore wind farm with 16 NREL 5 MW wind turbines is shown in Fig. 7.

2.5. Techno-economic model

The feasibility of an offshore wind farm project depends on its techno-economic Key Performance Indicators (KPIs). The Levelised Cost of Energy (LCOE) is used in this study to optimise the offshore wind farm layout as it considers the productivity and cost components of the project. The LCOE is expressed as

$$LCOE = \frac{CAPEX + \sum_{i=1}^{n} \frac{OPEX}{(1+r)^i} + \frac{D}{(1+r)^n}}{\sum_{i=1}^{n} \frac{AEP}{(1+r)^i}} \tag{17}$$

where *CAPEX*, *OPEX* and *D* are the CAPital EXpenditure (CAPEX), the Operating Expenditure (OPEX) and the decommissioning cost of the offshore wind farm; r is the Weighted Average Cost of Capital (WACC) and n is the project lifetime. The WACC is assumed as 10 % [70] and the project lifetime as 25 years [70]. OPEX specific cost is assumed for commercial scale as 0.09 M€/MW [59].

The CAPEX is obtained as

$$CAPEX = C_{Turb} + C_{Plat} + C_{Moor} + C_{Inst} + C_{Grid} \tag{18}$$

where C_{Turb} is the wind turbines cost including the towers, C_{Plat} is the floating platforms cost, C_{Moor} is the moorings cost, C_{Inst} is the installation cost and C_{Grid} is the grid connection cost. Specific cost of the wind turbine, platform and installation are shown in Table 3. C_{Turb}, C_{Plat}, C_{Moor} and C_{Inst} have been multiplied by a cost reduction factor C_R [20], accounting for the cost reduction due to the larger number of wind turbines. C_R is expressed as:

$$C_R = \left(\frac{2}{3} + \frac{1}{3} e^{-0.00174 \cdot N_T^2}\right) \tag{19}$$

C_{Moor} is calculated as

$$C_{Moor} = n_M \cdot (C_{Anchor} + c_M \cdot L_M) \cdot N_T \cdot C_R \tag{20}$$

where n_M is the number of mooring lines, C_{Anchor} is the anchor cost, c_M is the specific mooring line cost and L_M is the mooring length. Values for these parameters are shown in Table 4 while the dependence between the mooring length and the sea depth is shown in Fig. 8.

Grid connection costs (C_{Grid}) include both the collection and transmission system costs. Each wind turbine is assumed to include a transformer to step up to the Medium Voltage Alternating Current (MVAC) grid connection lines (33 kV) to efficiently transmit the power produced to the offshore substation. The offshore substation is connected to the onshore substation via High Voltage Alternating Current (HVAC) grid connection lines (132 kV), which minimises power losses. The onshore substation connects the electricity supplied by the offshore wind farm to the island's local grid connection, which is assumed to be in MVAC.

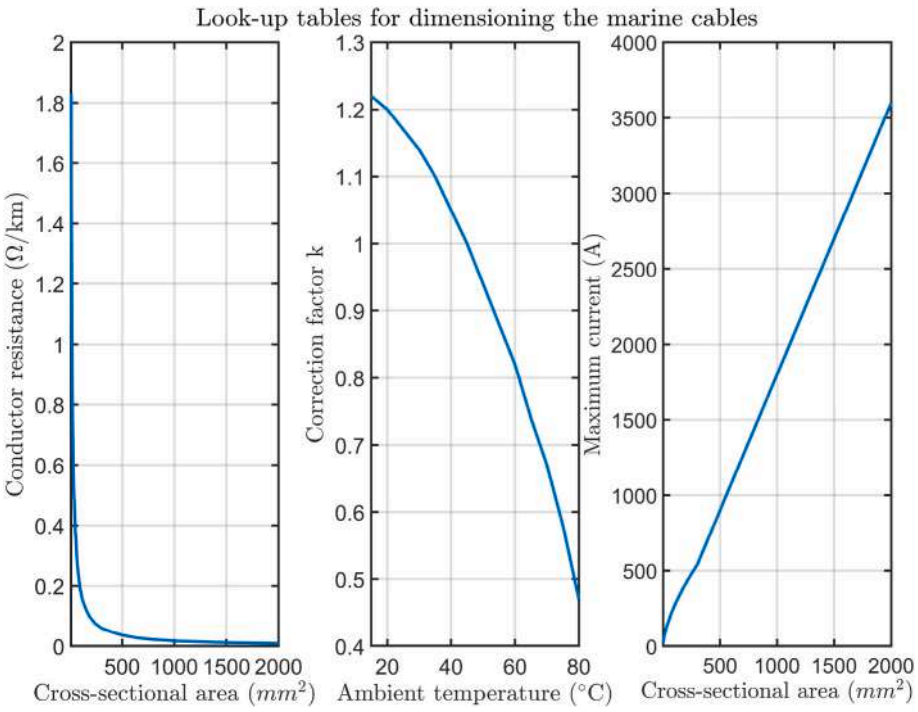

Fig. 6. Look-up tables for dimensioning the marine cables.

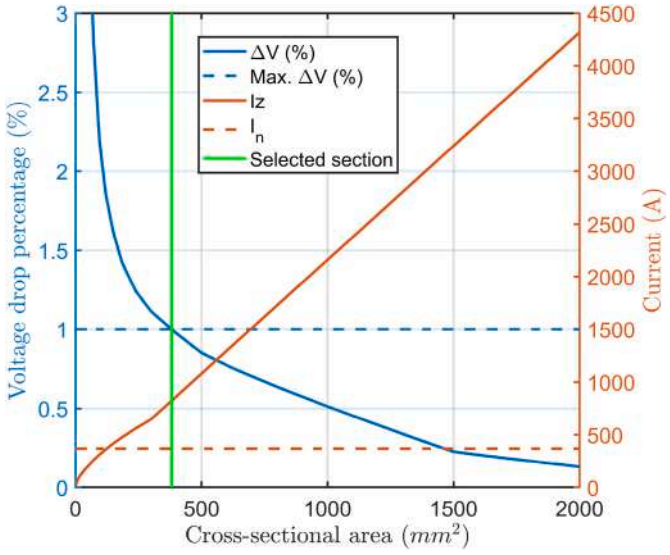

Fig. 7. Example of calculation of the cross-sectional area of the export cable for an offshore wind farm with 16 NREL 5 MW wind turbines.

The grid connection cost (C_{Grid}) is obtained from a cable cost model developed by Sharkey [65]. The cable cost is mainly influenced by the voltage rating, the cross-sectional area of the conductor, and the installation cost. It is obtained as

$$C_{Grid} = \sum_{i=1}^{N_T} \left(C_{int_i} + C_{dyn_i} + C_{con_i} \right) + C_{ex} + C_{Offsub} + C_{Onsub} \tag{21}$$

where C_{int} are the inter-array cable costs, C_{dyn} are the dynamic cable costs, C_{con} are the connector costs, C_{ex} are the export cable costs, C_{Offsub} and C_{Onsub} are the costs of the offshore and onshore substations.

C_{int} is obtained as

$$C_{int} = \left(C_{refC} \cdot f_S \cdot f_V + C_{refI} \cdot f_I \right) \cdot L_c \tag{22}$$

where C_{refC} is the reference inter-array cable specific cost (200 €/m for 95 mm^2 and 10 kV), C_{refI} is the reference inter-array installation cable specific cost (160 €/m for 95 mm^2 and 10 kV) and L_c is the inter-array cable length between each wind turbine and the offshore substation. f_S and f_V are the correction factors to account for a different section (f_S) and voltage (f_V) than the given reference. The installation specific cost is also corrected to consider the influence of section and voltage (f_I). The correction factors were obtained from the work of Sharkey and are shown in Fig. 9.

The specific cost of the dynamic cables (€/m) was considered as 50 % more expensive than the static cables [65] and it is calculated as

$$C_{dyn} = 1.5 \cdot \left(C_{refC} \cdot f_S \cdot f_V + C_{refI} \cdot f_I \right) \cdot L_{dyn} \tag{23}$$

where L_{dyn} is the length of each dynamic cable connecting the wind turbine to the seabed. L_{dyn} is assumed as the distance between the wind turbine rotor and the seabed.

Connector costs (C_{con}) are used to connect different parts of the electrical system to facilitate components and devices maintenance. We have assumed in this study wet-mate connectors with a cost of 0.3 M€/unit [65] that connect dynamic cables with the static cables.

Similarly, to C_{int}, the export cable costs (C_{ex}) are obtained as

$$C_{ex} = \left(C_{refC} \cdot f_S \cdot f_V + C_{refI} \cdot f_I \right) \cdot L_{ex} \tag{24}$$

where L_{ex} is the length of the export cable.

The offshore and onshore substation costs (C_{Offsub}, C_{Onsub}) are each estimated as the sum of the transformer and switchgear costs. The transformer cost is obtained as

$$C_{tr} = c_{tr1} \cdot P_{farm} \tag{25}$$

where c_{tr1} is assumed as 150.9 k€/MW and 21.56 k€/MW for the offshore and onshore transformer respectively [71] and P_{farm} is the farm rated power (MW). The switchgear cost is estimated as

$$C_{switch} = c_{s1} \cdot V_{HVAC} + c_{s2} \tag{26}$$

where c_{s1} and c_{s2} are respectively 0.668 €/V and 36000 € [72].

Table 3
Specific cost of CAPEX cost components.

		Specific cost (M€/MW)
Wind turbine		1.3 [70]
Platform	**Spar**	0.51 [59]
	Semi-submerged	0.65 [59]
Installation	**Spar**	0.42 [59]
	Semi-submerged	0.24 [59]

Table 4
Mooring line parameters [59,66].

	Hywind	WindFloat
Number of lines (n_M)	3	4
Anchor cost (C_{Anchor})	0.14 M€	0.07 M€
Mooring line specific cost (c_M)	500 €/m	500 €/m

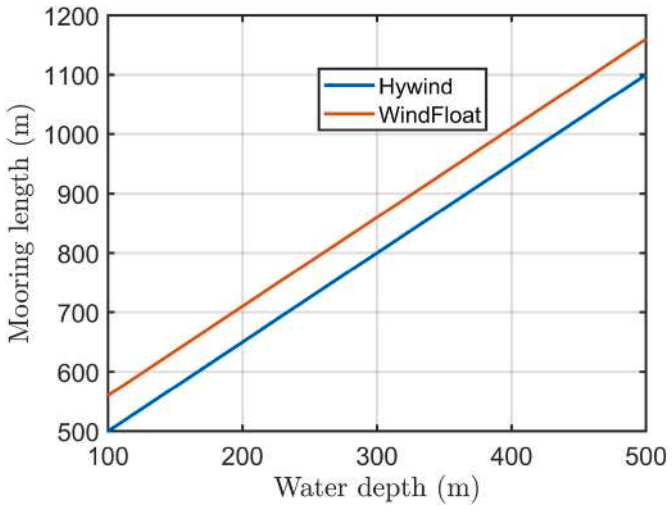

Fig. 8. Mooring line length as a function of water depth.

Finally, the decommissioning cost is obtained as

$$D = PF \cdot cc_{MW} \cdot (1 + cc_{cable}) \tag{27}$$

where cc_{MW} is assumed as 55 k€/MW and cc_{cable} is 12 % [33].

2.6. Layout optimisation

The layout optimisation is implemented for different types of wind turbines (5 MW and 15 MW), wind turbine number and site considered. The number of wind turbines is investigated between 4 and 24. The maximum number of 24 wind turbines was chosen to limit the computational time required to optimise the wind farm layout.

2.6.1. Problem variables

The optimisation variables of the study are the coordinates of the wind turbines and are twice the number of wind turbines. Therefore, the optimisation variables are:

$$x = \left[x_1, y_1, x_2, y_2, \ldots, x_{N_T}, y_{N_T}\right] \tag{28}$$

2.6.2. Constraints

The constraints of the optimisation are the minimum distance between the wind turbines and the wind farm limitation area. In general, a minimum distance between offshore wind turbines is recommended, which is generally at least four times the diameter [37,66], to avoid higher turbulence that could lead to structural and fatigue damage. Furthermore, the Jensen wake model [51] is a far-wake model that gives sensible results for minimum distances larger than four rotor diameters.

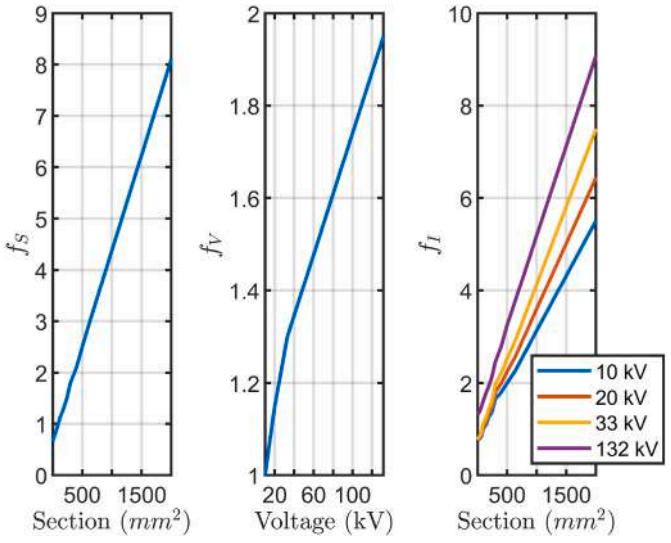

Fig. 9. Correction factors for the estimation of the cable specific cost [65].

For these reasons, a minimum distance of four rotor diameters between wind turbines was used in this study. The nonlinear constraint can be expressed as

$$\frac{\left(x_i - x_j\right)^2 + \left(y_i - y_j\right)^2}{(4D)^2} \geq 1; \forall i = 1, \ldots, (N_T - 1); \forall j > i \tag{29}$$

Wind turbines should be located within a predefined limitation area. The wind farm limitation area is assumed to have a square shape with two different square sizes of 2.5×2.5 km^2 and 5×5 km^2 chosen for the 5 MW and the 15 MW, respectively, to hold the maximum number of 24 wind turbines due to constraints. In fact, the rotor diameter of the IEA 15 MW is about double of the 5 MW (240 m and 126 m respectively), resulting in a similar maximum number of wind turbines. The constraint of the wind farm area limits is expressed as

$$\begin{cases} -\frac{S}{2} < x_i < \frac{S}{2} \\ -\frac{S}{2} < y_i < \frac{S}{2} \end{cases} \forall i = 1, \ldots, N_T \tag{30}$$

where S is the square side length.

2.6.3. Optimisation problem

The LCOE of the wind farm, defined in Equation (17), is the objective function of the layout optimisation, which accounts both the annual energy production and the total cost of the wind farm. The optimisation problem is described as

$$\underset{x}{minimise}\ LCOE(x) \tag{31}$$

subject to constraints (29) and (30).

If constraints are not verified for the *fminsearch* function (See Section 2.6.4), LCOE is obtained using a penalty function as follows:

$$LCOE = 500 + |D_{minF} - 4D| \tag{32}$$

where D_{minF} is the minimum distance between the wind turbines for each layout evaluated. The penalty function includes a large LCOE of 500 €/MWh and the difference between D_{minF} and the minimum constraint distance to penalise solutions with the minimum distance less than the constraint of 4D.

2.6.4. Optimisation algorithms

The optimisation problem of this study can be solved by several optimisation algorithms which can deal with linear and nonlinear inequality constraints and can search the global optimum. Stochastic optimisation algorithms can investigate the global optimum of an optimisation problem, while deterministic optimisation is generally limited to finding local optima. These algorithms can also be combined to achieve better performance by first using stochastic optimisation to explore the design space and identify the optimal region, and then using deterministic optimisation to refine the optimum, as it has a higher convergence rate. Another alternative for finding the global optimum is to repeat the deterministic optimisation algorithm several times with several initial starting guesses [37].

Different optimisation algorithms have been tested to check their optimisation efficiency and convergence rate to the optimal array configuration. The optimisation algorithm tested are the followings:

- *Iterative fminsearch (IFS)*
- *Iterative fmincon (IFC)*
- *Modified Genetic Algorithm + fminsearch (mGA)*

MATLAB functions such as *fminsearch* and *fmincon* are well-known MATLAB optimisation functions which can optimise complex optimisation problems. *fminsearch* is based on the Nelder-Mead simplex algorithm and is an efficient optimisation algorithm for unconstrained multivariable functions. The inclusion of mathematical programming techniques such as the MATLAB function *fmincon* in the optimisation approach has the benefit that can deal efficiently with nonlinear constraints such as the minimum distance constraint and can satisfy the Karush-Kuhn-Tucker optimality conditions, which adds robustness to the optimal results obtained [37]. *fmincon* was investigated using the default "interior-point" algorithm option. Both *fminsearch* and *fmincon* were evaluated for 5000 different layouts and repeated five times to check a larger set of local solutions. The starting guess of the *fminsearch* and *fmincon* algorithms was obtained from the best solution of an initial evaluation of 1000 random feasible solutions.

A modified *GA* combined with *fminsearch* (*mGA*) was also tested as it has demonstrated high optimisation convergence rate in previous works [73–77]. The *GA* was modified to include a radial basis surrogate model, which is an efficient surrogate model when the model is built on many solutions, e.g. compared to more computationally expensive surrogate models such as the Kriging. In the new generation, new individuals are partially chosen from the best surrogate solutions, which is set to 10 % in this study. GA is known to deal not efficiently with nonlinear constraints [19]. In this work, we have used a repairing action similar to Ref. [23], where unfeasible solutions are replaced by feasible ones. The *fminsearch* function is then used to optimise locally the solution found with the modified GA. The optimisation parameters are given in Table 5.

3. Results

3.1. Verification of the model

The in-house wind farm model was developed in MATLAB to allow coupling with the MATLAB optimisation algorithm developed in previous studies (See *mGA* in Section 2.6). Pywake was chosen as the reference code for validating the in-house code, as it is a well-known and established code developed by DTU [40]. Pywake is an open-source Python code able to simulate wind farms, and compute the *AEP* and the individual wind turbine power production. Pywake includes the possibility to choose between wake deficit models such as Jensen and Bastankhah wake models, superposition, blockage, rotor-average, deflection, turbulence, and ground models. In this work the Jensen wake deficit model, the Sum of Squares (SS) superposition, and the Area Overlapping rotor-average models are verified and compared between the in-house code and Pywake. Two different wind farm configurations were tested and compared between the two codes (See Fig. 10). The two codes are compared in terms of energy production for three different wind directions and 28 wind speeds across the operating working range. The energy production of the wind farm is the highest for both layouts when the wind direction is 0°; it decreases slightly for a wind direction of 60° and more significantly for 90°. In particular, the first layout is more influenced by the 90° wind direction as the shadowing effect is larger. The in-house code and Pywake show very similar results with a very small relative difference (about 0.0001 %). Finally, the in-house code demonstrated a higher computational efficiency (5–6 times faster) compared to Pywake, as Pywake probably simulates multiple subroutines which slows down the calculation.

3.2. Optimisation convergence

The efficiency of the proposed optimisation algorithm is tested for an optimisation case. The Chios site is chosen as the reference test, while 15 NREL 5 MW wind turbines are considered in the optimisation. A larger number of wind turbines is expected to increase the number of optimisation variables, but at the same time, the wind farm area becomes saturated, reducing the optimisation feasible solutions. Fig. 11 shows the convergence results for the optimisation algorithms explained in Section 2.6 and the optimal layout configurations of the wind farm. *mGA* has a lower optimisation convergence rate than the other two algorithms due to the low efficiency of the genetic algorithm. The convergence rate of *mGA* improves in the last part of the optimisation due to the higher convergence rate of *fminsearch*. *IFC* and *IFS* show a similar convergence rate efficiency, whose difference in the final optimum is due to the stochastic search of the initial guess, which affects less the optimum found when the number of iterative repetitions of *fmincon* and *fminsearch* is increased. *IFC* was selected to obtain the optimisation results of this study and was also tested for other three longer convergence tests (6500 algorithm iterations repeated seven times). The optimal LCOEs obtained with this algorithm are similar (0.5 % relative difference), which gives some confidence that an optimal global optimum is almost achieved. On the other hand, the optimised layout configuration (Fig. 11c and d) differs between the optimisations, suggesting that the global optimal layout configuration has probably not been achieved. However, this study aims to optimise the LCOE of the offshore wind farm and focuses less on the convergence of the wind farm layout configuration, which might require many more simulations. The computational time required for the long optimisation convergence test was about 3 h on an Intel(R) Core(TM) i9-9900K CPU @ 3.60 GHz processor and 32.0 GB installed memory.

3.3. Optimisation results

The optimal offshore wind farm layout configuration is investigated in terms of the number (4-24), type of wind turbines (5 MW and 15 MW), and site considered using the *IFC* optimisation algorithm with the longer optimisation convergence check settings. The main results are shown in Fig. 12 and Table 6. Fig. 12 shows the normalised optimal LCOE (nLCOE) and the normalised capacity factor (nCF) in relation to the maximum LCOE and CF, respectively, as a function of the number of wind turbines.

nLCOE and nCF are similar at the different sites, with a maximum difference of about 2–3 %. The lowest nLCOE as a function of the number of wind turbines is about 10 % lower compared to the highest nLCOE. The nLCOE of the NREL 5 MW reaches a minimum between 11 and 22 wind turbines and show a small variation in this range, as the optimal result probably does not fully converge to the optimal solution (section 3.2 has shown a difference of 0.5 % between the optimal LCOE solutions). The nLCOE of the IEA 15 MW shows a different influence on the turbine number compared to the optimal LCOE of the NREL 5 MW. For a small number of wind turbines, it is initially high due to the quick increase in HVAC cross-sectional area and then decreases reaching a

Table 5
Optimisation parameters for mGA.

GA population	750
GA generations	30
GA elitism factor surrogate	0.1
fminsearch	7500

minimum for the maximum feasible number of wind turbines (minimum LCOE for 22–24 wind turbines). Cable costs and HVAC cross-sectional area are shown in Fig. 13. All sites have similar cable costs and HVAC cross-sectional areas because the cables are designed based on the same rated power, voltage, and HVAC cable length.

The optimal nCF of the wind farm shows good optimisation convergence with the different number of wind turbines, as it is similar between all optimisations and is maximum up to 11–12 wind turbines as the wind farm minimises aerodynamic losses. Crete shows the least reduction in the wind farm capacity factor, as the wind at this location comes mainly from one direction (NW) and the optimal configuration reduces aerodynamic losses more efficiently (See Fig. 3). The nCF for Crete and 24 wind turbines is about 2 % larger compared to San Pietro and Korcula, which are characterised by a larger wind direction variability.

Table 6 shows that the lowest LCOE and the highest capacity factor are obtained for the most energetic sites such as Crete and Chios and the IEA 15 MW. In particular, the LCOE of the IEA 15 MW is generally 25 % lower than the NREL 5 MW. Korcula has the lowest optimal LCOE due to the lowest available average wind speed. Grid connection losses are generally low (around 0.1–0.3 %) and therefore have a minor impact on the capacity factor. The main cost in all cases is represented by the wind turbine cost, followed by the grid connection and platform costs. The number of wind turbines of 5 MW and 15 MW for Chios is limited by the island's electrical load capacity, as explained in Section 2.1, and is reduced to 15 and 5 respectively. For the 5 MW, it is slightly affected, while for the 15 MW, it remains at the highest LCOE and maximum capacity factor.

Figs. 14 and 15 show two optimal wind farm layouts for the Chios location. Fig. 14 shows the wakes generated by 16 NREL 5 MW wind turbines optimised to reduce aerodynamic losses. It is possible to observe that the wind turbines in the two main wind directions (0° and 180°), which generate the most power, produce the maximum possible power, and minimise power losses. Fig. 15 shows the optimal configuration of 4 NREL 5 MW wind turbines. The wind turbines minimise both aerodynamic losses and grid connection cost between the turbines, as they are located close to the substation minimising the MVAC cables length.

4. Discussion

The optimal LCOE of the floating offshore wind farms from this study demonstrates to be competitive with bottom-fixed offshore wind farms, especially in Crete, the most energetic location considered, where the LCOE reaches about 80 €/MWh for the 15 MW wind turbine [59]. San Pietro and Korcula resulted in a higher LCOE compared to Crete and Chios due to the lower average wind speed. In Refs. [11,78], the LCOE was mapped for the entire Mediterranean Sea. This study shows a similar

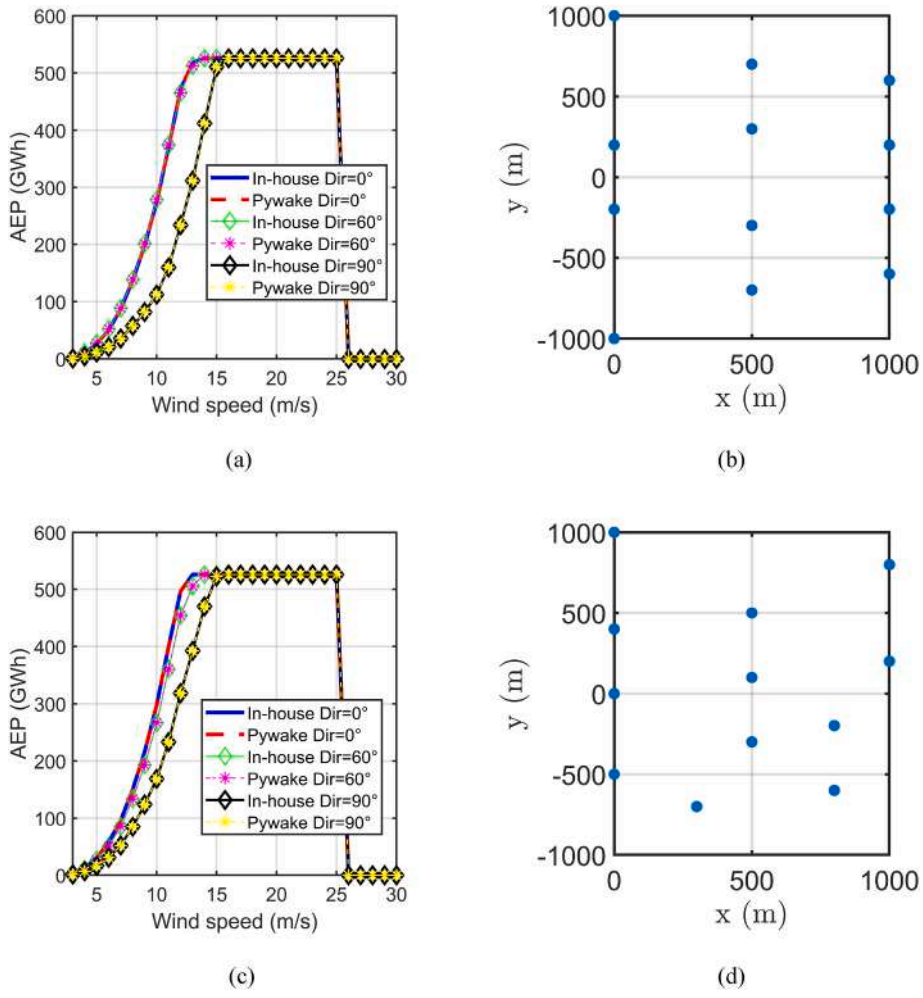

Fig. 10. Verification of the MATLAB in-house code with Pywake for layout 1 (a, b) and layout 2 (c, d). Wind direction is relative to the x axis.

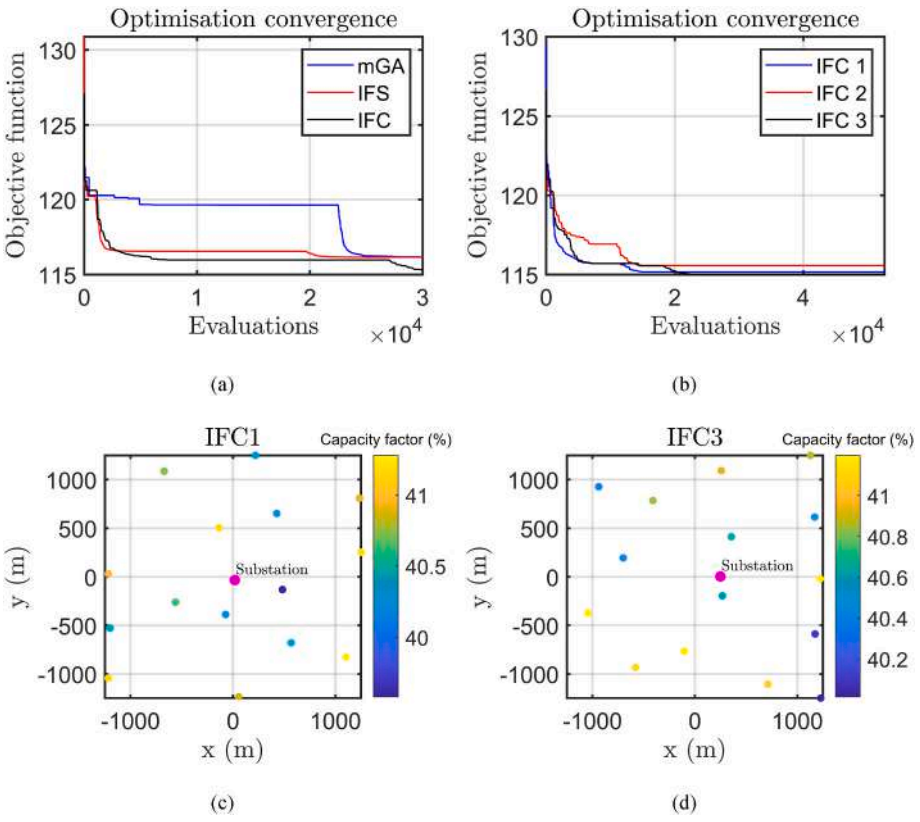

Fig. 11. Convergence results for three different optimisation algorithms (mGA, IFS and IFC) for the Chios site and 15 NREL 5 MW wind turbines (a) and for three different optimisations of IFC and longer convergence test (b). Optimal layout configuration of IFC1 (c) and IFC 3 (d).

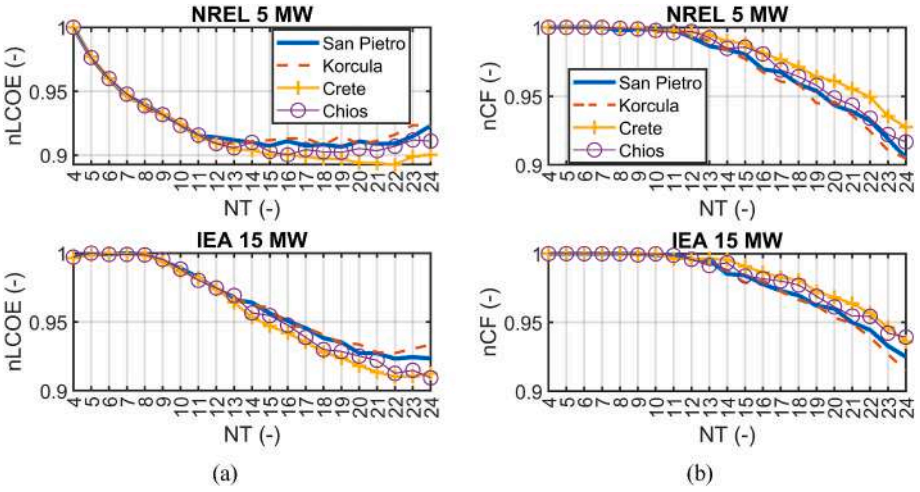

Fig. 12. Optimal nLCOE (a) and nCF (b) for the 5 MW and 15 MW and the locations considered.

LCOE comparison with [78] for the considered sites and the 5 MW wind turbine, although in Ref. [78] a wind farm with 200 turbines of 5 MW each was assumed. LCOE in Ref. [10] was lower compared to this study, as it was estimated for a future scenario in 2030. A significant reduction in LCOE can be expected if the HVAC power grid connection cable is nearby and already installed. Therefore, planned offshore wind farms close to existing wind farms lead to a significant LCOE reduction of up to 25 % when analysing the results of Table 6.

Similar to this study, it is found in Refs. [35,79] that increasing the size of wind turbines is more profitable than using smaller wind turbines. In this work, it is found that the LCOE is reduced by about 25 % choosing the IEA 15 MW instead of the NREL 5 MW.

For simplicity, the electrical connection between the arrays in this study is limited to a star configuration, which may not be the optimal solution for reducing costs and energy losses compared to a radial configuration [65]. Electrical grid layout optimisation has been included in the wind farm optimisation problem in Refs. [80–82], for example. In particular, the power flow problem was solved in Ref. [80] using the MATLAB package tool MATPOWER.

Grid connection cost is high due to the HVAC cable cost and has a significant impact on the LCOE. The HVAC cable's cross-sectional area reaches large values, as the voltage drop and maximum current must be kept below certain limits. It is expected that a change in these design parameters will significantly affect the optimal number of wind

Table 6
Optimal results of the location considered.

Wind turbines	San Pietro		Korcula		Crete		Chios	
	5 MW	15 MW	5 MW	15 MW	5 MW	15 MW	5 MW	15 MW
nTurb	19	22	18	22	22	22	16	24
LCOE (€/MWh)	162.5	118.1	192.9	137.6	108.1	80.0	114.7	84.8
CFfarm (%)	27.7	33.8	23.3	28.8	41.4	50.2	40.5	46.4
AEP (GWh)	230.4	978.1	184.1	831.5	399.1	1452.6	283.8	1462.9
Grid losses (%)	0.09	0.14	0.06	0.10	0.19	0.30	0.19	0.26
CAPEX (M€)	262.2	779.3	248.8	768.8	301.7	785.1	230.2	832.1
C_{Turb} **(M€)**	104.3	347.6	100.2	347.6	115.9	347.6	91.5	369.3
C_{Plat} **(M€)**	40.9	136.4	50.1	173.8	45.5	136.4	35.9	144.9
C_{Moor} **(M€)**	21.7	24.1	22.5	26.0	28.9	28.9	21.9	29.4
C_{Inst} **(M€)**	33.7	112.3	18.5	64.2	37.4	112.3	29.6	119.3
C_{Grid} **(M€)**	61.6	158.9	57.5	157.2	74.0	160.0	51.3	169.2
C_{ex} **(M€)**	30.4	70.2	28.5	70.2	36.8	70.2	24.7	72.2

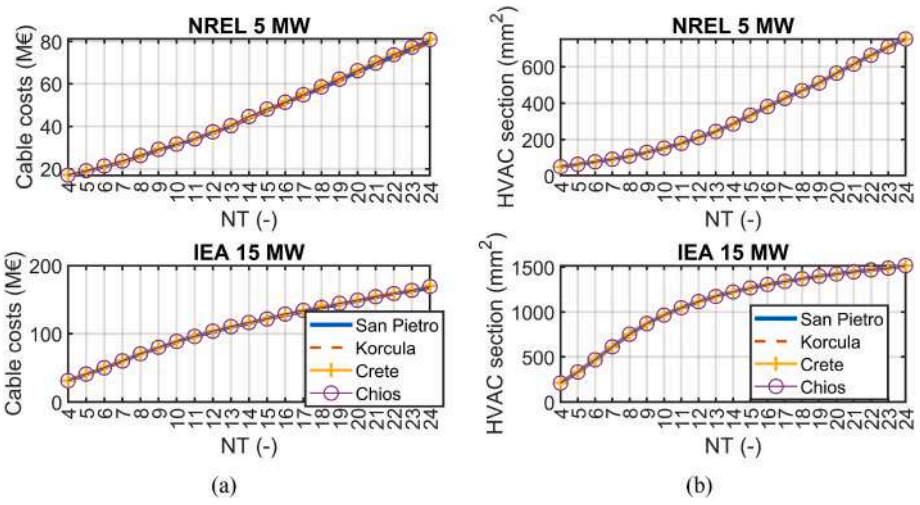

Fig. 13. Grid connection costs (a) and cross-sectional area of HVAC cables of the optimal configurations for the locations considered.

turbines. However, the optimal wind farm layout of the offshore wind farm is not influenced by the HVAC cable costs but minimises the aerodynamic losses and the MVAC cable costs.

The economy of scale influences the optimal LCOE depending on the number of wind turbines. In this study, following previous work [20,21], a cost reduction factor of one-third of the wind turbine costs was assumed for a larger number of wind turbines. The cost reduction factor should be further investigated and updated with a more reliable factor. The number of wind turbines found is also limited by the wind farm layout size and the maximum number of wind turbines considered, which is 24 in this study due to spatial constraint limits.

Several studies mainly considered the GA for wind farm layout optimisation [18] while only a few studies compared the convergence efficiency of different optimisation algorithms. In this study, GA showed a lower convergence rate compared to the other selected algorithms, as GA deals less efficiently with nonlinear constraints compared to *fminsearch* and *fmincon* [19]. In previous studies, GA was compared with PSO [28,34] and SA [26], and similarly to this study, GA was mostly outperformed by the newly proposed optimisation algorithms. The iterative repetition of *fmincon* starting from a random initial guess was already tested in Ref. [37] to improve the annual energy production of the Alpha Ventus offshore wind farm. This study confirmed the high efficiency of this algorithm for wind farm layout optimisation studies.

5. Conclusions

In this work, we have optimised a floating offshore wind farm for four different suitable sites in the Mediterranean, considering technical and spatial constraints. The selected sites are located near the Mediterranean islands of San Pietro, Korcula, Chios, and Crete, which are characterised by high cost of energy and fossil fuels consumption. Therefore, the development of an offshore wind farm will support the islands' transition to a more sustainable economy. This study also investigates the influence of the wind turbine type for a number between 4 and 24 wind turbines and considers a detailed techno-economic analysis to estimate the LCOE of the offshore wind farm, as it is the objective of the optimisation. The wake model was implemented in MATLAB and verified with the state-of-the-art code Pywake, the former having a higher computational efficiency (5–6 times). Optimisation algorithms for optimising the wind farm layout are compared and an efficient iterative repetition of the MATLAB function *fmincon* is preferred over a modified genetic algorithm (*mGA*) and the iterative MATLAB *fminsearch*.

The normalised optimal LCOE and the capacity factor as a function of the number of wind turbines are similar for the different sites and reach a maximum difference of 2–3 %, showing that they are not significantly affected by the resource. The wind turbine type has a significant influence on the optimal LCOE as a function of the number of wind turbines reaching a minimum between 12 and 22 wind turbines for the 5 MW wind turbine and between 22 and 24 for the 15 MW. The lowest optimal LCOE as a function of the number of wind turbines is about 10 % below the worst-case scenario with the highest number of wind turbines. In Crete, the reduction of the capacity factor is lower when the number of wind turbines is increased, as the wind rose is rather unidirectional, and therefore the optimal layout reduces the wake interactions more efficiently.

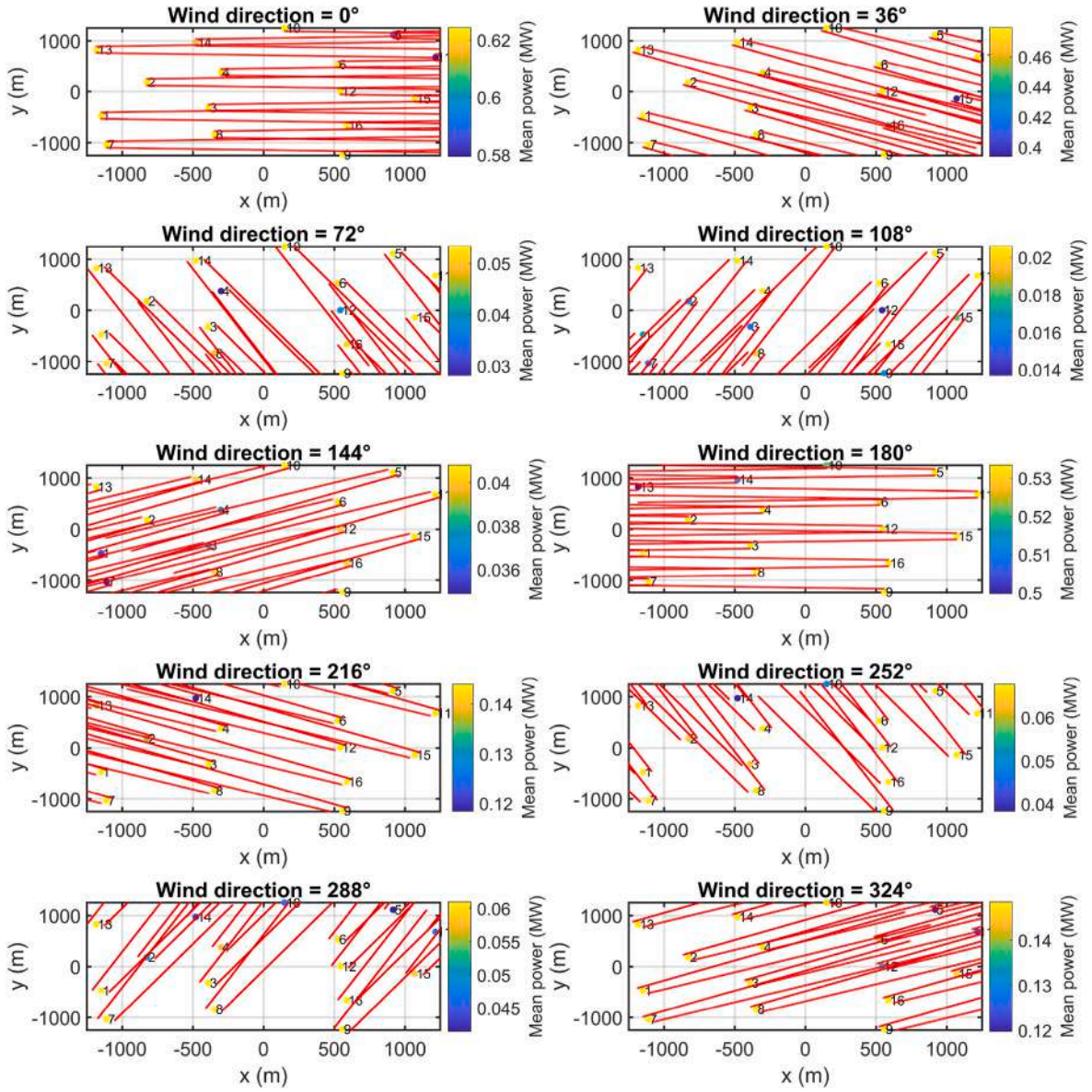

Fig. 14. Optimal offshore wind farm layout of the 5 MW wind turbine for Chios and 16 wind turbines. The wake of each wind turbine are visualized with a red line.

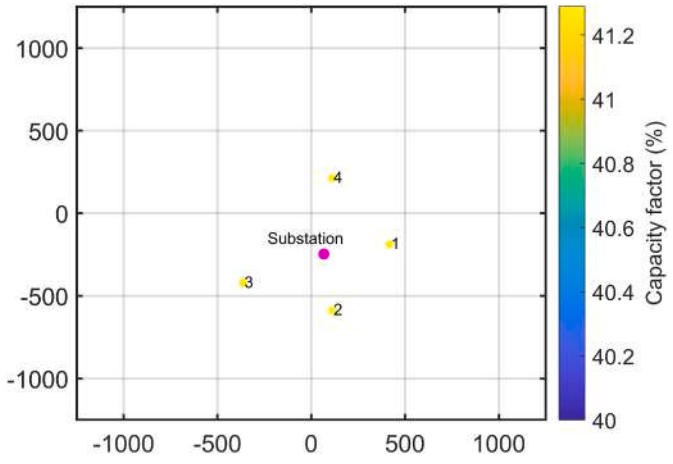

Fig. 15. Optimal offshore wind farm layout of the 5 MW wind turbine for Chios and 4 wind turbines.

Future work will include grid connection design parameters to optimise the offshore wind farm layout, such as the maximum allowable voltage drop. In addition, the radial configuration of the inter-array grid layout will be investigated and integrated into the optimisation, as it could reduce costs compared to the star configuration. Finally, future work will also investigate the influence of the wind farm layout size on the optimal installed wind turbine capacity per km^2.

CRediT authorship contribution statement

E. Faraggiana: Conceptualization, Methodology, Software, Data curation, Visualization, Formal analysis, Writing – original draft, Writing – review & editing. **A. Ghigo:** Writing – review & editing. **M. Sirigu:** Writing – review & editing. **E. Petracca:** Writing – review & editing. **G. Giorgi:** Writing – review & editing. **G. Mattiazzo:** Supervision, Project administration, Funding acquisition. **G. Bracco:** Conceptualization, Supervision, Project administration, Funding acquisition.

Declaration of competing interest

The authors declare that they have no known competing financial interests or personal relationships that could have appeared to influence the work reported in this paper.

References

[1] D. Groppi, A. Pfeifer, D.A. Garcia, G. Krajačić, N. Duić, A review on energy storage and demand side management solutions in smart energy islands, Renew. Sustain. Energy Rev. 135 (2021), 110183, https://doi.org/10.1016/j.rser.2020.110183.

[2] Z. Wang, R. Carriveau, D.S.-K. Ting, W. Xiong, Z. Wang, A review of marine renewable energy storage, Int. J. Energy Res. 43 (2019) 6108–6150, https://doi.org/10.1002/er.4444.

[3] UL Solutions Spain, H2OCEAN, CORDIS EU Research Results, 2014. https://cordis.europa.eu/project/id/288145. (Accessed 11 August 2023).

[4] EU Commission, MERMAID, 2015. https://cordis.europa.eu/project/id/288710.

[5] PLOCAN, TROPOS, CORDIS EU Research Results, 2015. https://cordis.europa.eu/project/id/288192. (Accessed 11 August 2023).

[6] A. Babarit, J.-C. Gilloteaux, G. Clodic, M. Duchet, A. Simoneau, M.F. Platzer, Techno-economic feasibility of fleets of far offshore hydrogen-producing wind energy converters, Int. J. Hydrogen Energy 43 (2018) 7266–7289, https://doi.org/10.1016/j.ijhydene.2018.02.144.

[7] R. Loisel, L. Baranger, N. Chemouri, S. Spinu, S. Pardo, Economic evaluation of hybrid off-shore wind power and hydrogen storage system, Int. J. Hydrogen Energy 40 (2015) 6727–6739, https://doi.org/10.1016/j.ijhydene.2015.03.117.

[8] D. Milone, D. Curto, V. Franzitta, A. Guercio, M. Cirrincione, A. Mohammadi, An economic approach to size of a renewable energy mix in small Islands, Energies 15 (2005), https://doi.org/10.3390/en15062005, 2022.

[9] A. Pfeifer, V. Dobravec, L. Pavlinek, G. Krajačić, N. Duić, Integration of renewable energy and demand response technologies in interconnected energy systems, Energy 161 (2018) 447–455, https://doi.org/10.1016/j.energy.2018.07.134.

[10] M. Rava, P. Dafnakis, V. Martini, G. Giorgi, V. Orlando, G. Mattiazzo, G. Bracco, A. Gulisano, Low-cost heaving single-buoy wave-energy point absorber optimization for Sardinia west coast, J. Mar. Sci. Eng. 10 (2022) 397, https://doi.org/10.3390/jmse10030397.

[11] I. Kielichowska, K. Staschus, A.V. Lejarreta, L. Sijtsma, L. Ramaekers, B. Vree, G. R. Yeomans, C. Wouters, S. Lindroth, F. Krönert, Study on the Offshore Grid Potential in the Mediterranean Region, 2020. Brussels.

[12] A. Ghigo, E. Faraggiana, M. Sirigu, G. Mattiazzo, G. Bracco, Design and analysis of a floating photovoltaic system for offshore installation: the case study of lampedusa, Energies 15 (2022) 8804, https://doi.org/10.3390/en15238804.

[13] A. Sahu, N. Yadav, K. Sudhakar, Floating photovoltaic power plant: a review, Renew. Sustain. Energy Rev. 66 (2016) 815–824, https://doi.org/10.1016/j.rser.2016.08.051.

[14] F. Onea, E. Rusu, A spatial analysis of the offshore wind energy potential related to the Mediterranean islands, Energy Rep. 8 (2022) 99–105, https://doi.org/10.1016/j.rser.2016.08.051.

[15] M.M. Nezhad, M. Neshat, D. Groppi, P. Marzialetti, A. Heydari, G. Sylaios, D. A. Garcia, A primary offshore wind farm site assessment using reanalysis data: a case study for Samothraki island, Renew. Energy 172 (2021) 667–679, https://doi.org/10.1016/j.renene.2021.03.045.

[16] H. Stančin, A. Pfeifer, C. Perakis, N. Stefanatos, M. Damasiotis, S. Magaudda, F. Di Pietrantonio, H. Mikulcic, Blue energy spearheading the energy transition: the case of Crete, Front. Energy Res. (2022) 584, https://doi.org/10.3389/fenrg.2022.868334.

[17] F. Cassola, M. Burlando, M. Antonelli, C.F. Ratto, Optimization of the regional spatial distribution of wind power plants to minimize the variability of wind energy input into power supply systems, J. Appl. Meteorol. Climatol. 47 (2008) 3099–3116, https://doi.org/10.1175/2008JAMC1886.1.

[18] R. Shakoor, M.Y. Hassan, A. Raheem, Y.-K. Wu, Wake effect modeling: a review of wind farm layout optimization using Jensen′ s model, Renew. Sustain. Energy Rev. 58 (2016) 1048–1059, https://doi.org/10.1016/j.rser.2015.12.229.

[19] M. Samorani, The Wind Farm Layout Optimization Problem, Handb. Wind Power Syst., 2013, pp. 21–38.

[20] G. Mosetti, C. Poloni, B. Diviacco, Optimization of wind turbine positioning in large windfarms by means of a genetic algorithm, J. Wind Eng. Ind. Aerod. 51 (1994) 105–116, https://doi.org/10.1016/0167-6105(94)90080-9.

[21] S.A. Grady, M.Y. Hussaini, M.M. Abdullah, Placement of wind turbines using genetic algorithms, Renew. Energy 30 (2005) 259–270, https://doi.org/10.1016/j.renene.2004.05.007.

[22] U.A. Ozturk, B.A. Norman, Heuristic methods for wind energy conversion system positioning, Elec. Power Syst. Res. 70 (2004) 179–185, https://doi.org/10.1016/j.epsr.2003.12.006.

[23] A.M. Abdelsalam, M.A. El-Shorbagy, Optimization of wind turbines siting in a wind farm using genetic algorithm based local search, Renew. Energy 123 (2018) 748–755, https://doi.org/10.1016/j.renene.2018.02.083.

[24] A. Kusiak, Z. Song, Design of wind farm layout for maximum wind energy capture, Renew. Energy 35 (2010) 685–694, https://doi.org/10.1016/j.renene.2009.08.019.

[25] R.A. Rivas, J. Clausen, K.S. Hansen, L.E. Jensen, Solving the turbine positioning problem for large offshore wind farms by simulated annealing, Wind Eng. 33 (2009) 287–297, https://doi.org/10.1260/0309-524X.33.3.287.

[26] J.-F. Herbert-Acero, J.-R. Franco-Acevedo, M. Valenzuela-Rendón, O. Probst-Oleszewski, Linear wind farm layout optimization through computational intelligence, in: MICAI 2009 Adv. Artif. Intell. 8th Mex. Int. Conf. Artif. Intell. Guanajuato, México, Novemb. 9-13, 2009. Proc, vol. 8, 2009, pp. 692–703.

[27] R. Rahmani, A. Khairuddin, S.M. Cherati, H.A.M. Pesaran, A novel method for optimal placing wind turbines in a wind farm using particle swarm optimization (PSO), in: 2010 Conf. Proc. IPEC, 2010, pp. 134–139.

[28] S. Pookpunt, W. Ongsakul, Optimal placement of wind turbines within wind farm using binary particle swarm optimization with time-varying acceleration coefficients, Renew. Energy 55 (2013) 266–276, https://doi.org/10.1016/j.renene.2012.12.005.

[29] Y. Eroglu, S.U. Seçkiner, Design of wind farm layout using ant colony algorithm, Renew. Energy 44 (2012) 53–62, https://doi.org/10.1016/j.renene.2011.12.013.

[30] S. Sisbot, Ö. Turgut, M. Tunç, Ü. Çamdali, Optimal positioning of wind turbines on Gökçeada using multi-objective genetic algorithm, Wind Energy An Int. J. Prog. Appl. Wind Power Convers. Technol. 13 (2010) 297–306, https://doi.org/10.1002/we.339.

[31] A. Emami, P. Noghreh, New approach on optimization in placement of wind turbines within wind farm by genetic algorithms, Renew. Energy 35 (2010) 1559–1564, https://doi.org/10.1016/j.renene.2009.11.026.

[32] P.P. Biswas, P.N. Suganthan, G.A.J. Amaratunga, Decomposition based multi-objective evolutionary algorithm for windfarm layout optimization, Renew. Energy 115 (2018) 326–337, https://doi.org/10.1016/j.renene.2017.08.041.

[33] C.N. Elkinton, Offshore Wind Farm Layout Optimization, PhD Thesis, University of Massachusetts Amherst, 2007.

[34] A.C. Pillai, J. Chick, M. Khorasanchi, S. Barbouchi, L. Johanning, Application of an offshore wind farm layout optimization methodology at Middelgrunden wind farm, Ocean Eng. 139 (2017) 287–297, https://doi.org/10.1016/j.oceaneng.2017.04.049.

[35] P. Ziyaei, M. Khorasanchi, H. Sayyaadi, A. Sadollah, Minimizing the levelized cost of energy in an offshore wind farm with non-homogeneous turbines through layout optimization, Ocean Eng. 249 (2022), 110859, https://doi.org/10.1016/j.oceaneng.2022.110859.

[36] S.D.O. Turner, D.A. Romero, P.Y. Zhang, C.H. Amon, T.C.Y. Chan, A new mathematical programming approach to optimize wind farm layouts, Renew. Energy 63 (2014) 674–680, https://doi.org/10.1016/j.renene.2013.10.023.

[37] B. Pérez, R. Minguez, R. Guanche, Offshore wind farm layout optimization using mathematical programming techniques, Renew. Energy 53 (2013) 389–399, https://doi.org/10.1016/j.renene.2012.12.007.

[38] P.Y. Zhang, D.A. Romero, J.C. Beck, C.H. Amon, Solving wind farm layout optimization with mixed integer programs and constraint programs, EURO J. Comput. Optim. 2 (2014) 195–219, https://doi.org/10.1007/s13675-014-0024-5.

[39] J.Y.J. Kuo, D.A. Romero, C.H. Amon, A mechanistic semi-empirical wake interaction model for wind farm layout optimization, Energy 93 (2015) 2157–2165, https://doi.org/10.1016/j.energy.2015.10.009.

[40] PyWake Dtu. https://topfarm.pages.windenergy.dtu.dk/PyWake/, 2023. (Accessed 1 February 2023).

[41] European Commission, Clean Energy Vision to Clean Energy Action, 2023. https://clean-energy-islands.ec.europa.eu/. (Accessed 10 January 2023).

[42] A. Vargiu, R. Novo, C. Moscoloni, E. Giglio, G. Giorgi, G. Mattiazzo, An energy cost assessment of future energy scenarios: a case study on san Pietro island, Energies 15 (2022) 4535, https://doi.org/10.3390/en15134535.

[43] Viohalco, Successful Completion of the Record-Breaking Crete Interconnection, 2023. https://www.viohalco.com/Article/108/. (Accessed 27 July 2023).

[44] Clean Energy for EU Islands, Chios, 2023. https://clean-energy-islands.ec.europa.eu/countries/greece/chios. (Accessed 26 July 2023).

[45] Emodnet, European Marine Observation and Data Network, 2023. https://emodnet.ec.europa.eu/geoviewer/. (Accessed 9 January 2023).

[46] DTU Wind Energy, Global Wind Atlas, 2023. https://globalwindatlas.info/en. (Accessed 5 May 2023).

[47] ERANET+ Project, New European Wind Atlas, 2023. https://map.neweuropeanwindatlas.eu/. (Accessed 13 January 2023).

[48] Wikipedia, List of Countries by Electricity Consumption, 2023. https://en.wikipedia.org/wiki/List_of_countries_by_electricity_consumption. (Accessed 9 January 2023).

[49] G. Cervelli, L. Parrinello, C. Moscoloni, G. Giorgi, Comparison of the ERA5 wave forecasting dataset against buoy record, Instrum. Mes. Métrol. 21 (2022), https://doi.org/10.18280/i2m.210301.

[50] D.J. Renkema, Validation of Wind Turbine Wake Models: Using Wind Farm Data and Wind Tunnel Measurements, Master's Thesis, TU Delft, 2007.

[51] N.O. Jensen, A Note on Wind Generator Interaction, Citeseer, 1983.

[52] I. Katic, J. Højstrup, N.O. Jensen, A Simple Model for Cluster Efficiency, Eur. Wind Energy Assoc. Conf. Exhib., Rome, 1986, pp. 407–410.

[53] J. Feng, W.Z. Shen, Solving the wind farm layout optimization problem using random search algorithm, Renew. Energy 78 (2015) 182–192, https://doi.org/10.1016/j.renene.2015.01.005.

[54] Diego Assencio, The Intersection Area of Two Circles, 2023. https://diego.assencio.com/?index=8d6ca3d82151bad815f78addf9b5c1c6. (Accessed 12 January 2023).

[55] W. Musial, B. Ram, Large-scale Offshore Wind Power in the United States: Assessment of Opportunities and Barriers, 2010.

[56] E. Faraggiana, G. Giorgi, M. Sirigu, A. Ghigo, G. Bracco, G. Mattiazzo, A review of numerical modelling and optimisation of the floating support structure for offshore wind turbines, J. Ocean Eng. Mar. Energy. (2022) 1–24, https://doi.org/10.1007/s40722-022-00241-2.

[57] J. Jonkman, Definition of the Floating System for Phase IV of OC3, 2010.

[58] D. Roddier, C. Cermelli, A. Aubault, A. Weinstein, WindFloat, A floating foundation for offshore wind turbines, J. Renew. Sustain. Energy 2 (2010), 33104, https://doi.org/10.1063/1.3435339.
[59] R. James, M.C. Ros, Floating Offshore Wind: Market and Technology Review, The Carbon Trust, 2015. https://www.carbontrust.com/our-work-and-impact/guides-reports-and-tools/floating-offshore-wind-market-technology-review. (Accessed 17 August 2023).
[60] J. Jonkman, S. Butterfield, W. Musial, G. Scott, Definition of a 5-MW Reference Wind Turbine for Offshore System Development, National Renewable Energy Lab, Golden, CO (United States), 2009. https://www.nrel.gov/docs/fy09osti/38060.pdf. (Accessed 17 August 2023).
[61] E. Gaertner, J. Rinker, L. Sethuraman, F. Zahle, B. Anderson, G.E. Barter, N. J. Abbas, F. Meng, P. Bortolotti, W. Skrzypinski, Others, IEA Wind TCP Task 37: Definition of the IEA 15-megawatt Offshore Reference Wind Turbine, 2020.
[62] NREL, OpenFAST. https://github.com/OpenFAST, 2023. (Accessed 1 February 2023).
[63] Renewables Now, Unitech to Take over Equinor's Hywind Demo off Norway, 2019. https://renewablesnow.com/news/unitech-to-take-over-equinors-hywind-demo-off-norway-638882/. (Accessed 21 January 2022).
[64] Offshore Wind, Principle power and mitsui bolster WindFloat tie-up in Japan (n.d.) https://www.offshorewind.biz/2017/05/03/principle-power-and-mitsui-bolster-windfloat-tie-up-in-japan/ (accessed 20 January 2023).
[65] F. Sharkey, Offshore Electrical Networks and Grid Integration of Wave Energy Converter Arrays-Techno-Economic Optimisation of Array Electrical Networks, Power Quality Assessment, and Irish Market Perspectives, PhD Thesis, Technological University Dublin, 2015.
[66] C. Bjerkseter, A. Agotnes, Levelised Cost of Energy for Offshore Wind Turbine Concepts, Master's Thesis, Norwegian University of Life Sciences, Ås, 2013.
[67] T. Wildi, Electrical Machines, Drives, and Power Systems, Pearson Educación, 2006.
[68] IEC, IEC 60228, 2023. https://webstore.iec.ch/publication/1065. (Accessed 17 January 2023).
[69] Cable Services, Cable Catalogue, 2023. https://www.cableservice.com/products. (Accessed 17 January 2023).
[70] Fundació Institut de Recerca en Energia de Catalunya, Deliverable 2.2, LCOE Tool Description, Technical and Environmental Impact Evaluation Procedure, LIFES50+ project, 2015. https://lifes50plus.eu/results/. (Accessed 17 August 2023).
[71] A.J. Collin, A.J. Nambiar, D. Bould, B. Whitby, M.A. Moonem, B. Schenkman, S. Atcitty, P. Chainho, A.E. Kiprakis, Electrical components for marine renewable energy arrays: a techno-economic review, Energies 10 (2017) 1973, https://doi.org/10.3390/en10121973.
[72] J.F. Herbert-Acero, O. Probst, P.-E. Réthoré, G.C. Larsen, K.K. Castillo-Villar, A review of methodological approaches for the design and optimization of wind farms, Energies 7 (2014) 6930–7016, https://doi.org/10.3390/en7116930.
[73] E. Faraggiana, J.C. Chapman, A.J. Williams, C. Whitlam, I. Masters, Investigation of new layout design concepts of an array-on-device WaveSub device, Renew. Energy 190 (2022) 501–523, https://doi.org/10.1016/j.renene.2022.03.126.
[74] E. Faraggiana, M. Sirigu, A. Ghigo, G. Bracco, G. Mattiazzo, An optimal design of the Hexafloat floating platform for offshore wind turbines, Trends Renew. Energies Offshore. (2022) 469–476.
[75] E. Amini, H. Mehdipour, E. Faraggiana, D. Golbaz, G.M.S. Bracco, M. Neshat, Optimization of hydraulic power take-off system settings for point absorber wave energy converter, Renew. Energy 194 (2022) 938–954, https://doi.org/10.1016/j.renene.2022.05.164.
[76] E. Faraggiana, I. Masters, J. Chapman, Design of an optimization scheme for the wavesub array, in: Proc. 3rd Int. Conf. Renew. Energies Offshore, 2018. Lisbon, Port.
[77] E. Faraggiana, M. Sirigu, A. Ghigo, G. Bracco, G. Mattiazzo, An efficient optimisation tool for floating offshore wind support structures, Energy Rep. 8 (2022) 9104–9118, https://doi.org/10.1016/j.egyr.2022.07.036.
[78] A. Martinez, G. Iglesias, Multi-parameter analysis and mapping of the levelised cost of energy from floating offshore wind in the Mediterranean Sea, Energy Convers. Manag. 243 (2021), 114416, https://doi.org/10.1016/j.enconman.2021.114416.
[79] I. Mustakerov, D. Borissova, Wind turbines type and number choice using combinatorial optimization, Renew. Energy 35 (2010) 1887–1894, https://doi.org/10.1016/j.renene.2009.12.012.
[80] L. Amaral, R. Castro, Offshore wind farm layout optimization regarding wake effects and electrical losses, Eng. Appl. Artif. Intell. 60 (2017) 26–34, https://doi.org/10.1016/j.engappai.2017.01.010.
[81] Y.-K. Wu, C.-Y. Lee, C.-R. Chen, K.-W. Hsu, H.-T. Tseng, Optimization of the wind turbine layout and transmission system planning for a large-scale offshore windfarm by AI technology, IEEE Trans. Ind. Appl. 50 (2013) 2071–2080.
[82] P. Hou, W. Hu, M. Soltani, Z. Chen, Optimized placement of wind turbines in large-scale offshore wind farm using particle swarm optimization algorithm, IEEE Trans. Sustain. Energy 6 (2015) 1272–1282.